



Self-Organization and Charge Transport Properties of Selenium and Tellurium Analogues of Polythiophene

Shuyang Ye, Lukasz Janasz, Wojciech Zajaczkowski, Joseph G. Manion, Anirban Mondal, Tomasz Marszalek, Denis Andrienko, Klaus Müllen, Wojciech Pisula,* and Dwight S. Seferos*

A series of conjugated polymers comprising polythiophene, polyselenophene, and polytellurophene with branched 3,7-dimethyloctyl side chains, well-matched molecular weight, dispersity, and regioregularity is synthesized. The ionization potential is found to vary from 5.14 to 5.32 eV, with polytellurophene having the lowest potential. Field-effect transistors based on these materials exhibit distinct hole transport mobility that varies by nearly three orders of magnitude, with polytellurophene having the highest mobility ($2.5 \times 10^{-2} \text{ cm}^2 \text{ V}^{-1} \text{ s}^{-1}$). The large difference in mobility demonstrates the significant impact of heteroatom substitution. Although the series of polymers are very similar in structure, their solid-state properties are different. While the thin film microstructure of polythiophene and polyselenophene is identical, polytellurophene reveals globular features in the film topography. Polytellurophenes also appear to be the least crystalline, even though their charge transport properties are superior to other samples. The torsional barrier and degree of planarity between repeat units increase as one moves down group-16 elements. These studies show how a single atom in a polymer chain can have a substantial influence on the bulk properties of a material, and that heavy group-16 atoms have a positive influence on charge transport properties when all other variables are kept unchanged.

The study of charge transport in π -conjugated polymers continues to be an area of intense materials chemistry research.^[1] These disordered organic semiconductors behave differently than their ordered inorganic counterparts. Early work focused on regioregular poly(3-alkylthiophene)s (P3ATs) (such as poly(3-hexylthiophene) [P3HT]) because these polymers readily form polycrystalline films, which were thought to be essential for achieving high charge carrier mobility. Indeed, P3HT and close analogues like poly(3,3'-dodecylquaterthiophene) achieved the highest mobility at that time, on the order of $10^{-1} \text{ cm}^2 \text{ V}^{-1} \text{ s}^{-1}$.^[2]

More recently, new classes of polymers such as *N*-alkyl dithieno[3,2-*b*:2',3'-*d*]pyrroles (DTP)-thiophene copolymers,^[3] benzothiadiazole-cyclopentadithiophene copolymers,^[4] 1,4-diketopyrrolo[3,4-*c*]pyrrole (DPP)-thieno[3,2-*b*]thiophene copolymers,^[5] indaceno-dithiophene-benzothiadiazole (C_{16} DT-BT) copolymers and 3-hexylthiophene-thiophene copolymers began to emerge that have mobilities exceeding that of P3HT.^[6] This is somewhat surprising given that these polymers have similar HOMO-LUMO bandgaps to P3HT and are overall less crystalline. In general, striking a balance between disorder and aggregation leading to better chain-chain coupling is thought to lead to enhanced transport properties.^[7]

With regard to consistent structure and properties, P3ATs are prime examples of polymers that can be prepared with precise length, dispersity, sequence and end groups.^[8] While their performance has been usurped by more elaborate donor-acceptor (D-A) type polymers,^[9] P3ATs still reign supreme in terms of controlled synthesis. Valiant efforts by some laboratories to control the chain length of D-A polymers using the Carothers equation model should be noted.^[10] However, P3ATs remain the only conjugated polymers that are synthesized in a controlled manner.

Recent efforts to extend P3ATs to more high-performance materials have focused on the use of other heterocycles. Poly(3-alkylselenophene)s (P3ASs) for example were first reported by Heeney et al.^[11] and have inspired work on heavier analogues of thiophene containing polymers.^[12] The selenium analogues

S. Ye, J. G. Manion, Prof. D. S. Seferos
Lash Miller Chemical Laboratory
University of Toronto
80 St. George Street, Toronto, Ontario M5S 3H6, Canada
E-mail: dseferos@chem.utoronto.ca

L. Janasz, Dr. T. Marszalek, Prof. W. Pisula
Department of Molecular Physics
Faculty of Chemistry
Lodz University of Technology
Zeromskiego 116, 90-924 Lodz, Poland
E-mail: pisula@mpip-mainz.mpg.de

W. Zajaczkowski, Dr. A. Mondal, Dr. T. Marszalek, Dr. D. Andrienko,
Prof. K. Müllen, Prof. W. Pisula
Max Planck Institute for Polymer Research
Ackermannweg 10, 55128 Mainz, Germany

Prof. D. S. Seferos
Department of Chemical Engineering and Applied Chemistry
University of Toronto
200 College Street, Toronto, Ontario M5S 3E5, Canada

The ORCID identification number(s) for the author(s) of this article can be found under <https://doi.org/10.1002/marc.201800596>.

DOI: 10.1002/marc.201800596

are more polarizable, have a higher dielectric constant, and stronger Se–Se interaction that should promote better chain–chain coupling, all of which should be advantageous for charge transport. By the time of writing certain selenophene-containing polymers now out-perform their thiophene counterparts.^[13] Notable examples include high performance n-channel polymers reported by Jenekhe, organic photovoltaic polymers from McCulloch and others.^[14] In addition to their homopolymers, selenophene and tellurophene are also widely utilized as flanking units in numerous high performance small molecules and copolymers, including D-A polymers.^[14b,15] The Seferos group has focused on the heaviest group-16 heterocycle, tellurophene.^[16] Although efforts to synthesize tellurophene polymers appeared in the literature as early as 1985,^[17] their controlled synthesis was only developed a few years ago.^[18]

Despite many recent advances in the synthesis of more and more challenging polymers that contain main group elements, an understanding of their material properties does not always keep up with the synthetic advances. Here we describe our initial attempts to establish structure-property relationships for regioregular tellurium and selenium analogues of poly(3-alkylthiophene)s. The poly(3-alkylthiophene) was prepared and serves as an important reference in this study. To make the compound labels clearer the tellurium-, selenium-, and sulfur-containing polymers will be referred to as PTe, PSe, and PTh, respectively. All samples have a very similar high molecular weight, narrow dispersity, identical side chains, and high regioregularity. We focus on the unique charge transport of each of the samples and how it relates to crystallinity, film morphology, HOMO-LUMO band-gap, and the predicted polymer confirmation.

For this study, monomers were designed to yield polymers with good solubility and processibility at molecular weights ($M_n \approx 30$ kDa) generally thought to have high charge carrier mobilities.^[19] Whereas P3HTs are quite soluble at these

molecular weights, solubility diminishes as one moves to larger heteroatoms. To solve this issue, we used larger, branched 3,7-dimethyloctyl (DMO) side chains. From a molecular design standpoint, the DMO side chain is seldom used in homopolymers or copolymers; however, it is commercially available (as the alcohol) and provides considerable solubility due to the two branching points.

The three polymers were synthesized by the catalyst transfer polycondensation (CTP) method, starting from the dihalogenated species. Briefly, the dihalogenated compounds were activated with isopropylmagnesium chloride and treated with Ni(dppe)Cl₂ (Figure 1a). The polymerizations were carried out with the same monomer:catalyst ratio (150:1). Due to the quasi-living character, one nickel catalyst initiates one polymer chain that propagates resulting in all three polymers having a very similar degree of polymerization or polymer length.

Further support of the controlled nature of the polymerization comes from gel permeation chromatography (GPC) analysis relative to polystyrene standards (Figure 1b, Figure S1, Table S1, Supporting Information). While GPC tends to overestimate the absolute molecular weight of conjugated polymers,^[20] it is useful for determining their relative elution volumes and hydrodynamic radii. The GPC-determined relative molecular weight is consistent with the monomer:catalyst ratio. This relative measurement shows that the polymers are similar in size and degree of polymerization. The dispersities (\mathcal{D}) of all polymers are as low as 1.2 indicating the chain lengths in one polymer sample vary over a narrow range of molecular masses.

In addition to molecular weight and \mathcal{D} ,^[19a,21] the regioregularity of a conjugated polymer has been shown to greatly impact the morphology and properties.^[22] To compare the effects of different heteroatoms (S, Se, Te), similar regioregularity is required. Due to the high monomer selectivity, CTP conditions produce polymers with almost pure head-to-tail linkages. Theoretically, the only tail-to-tail defect originates from the initiation

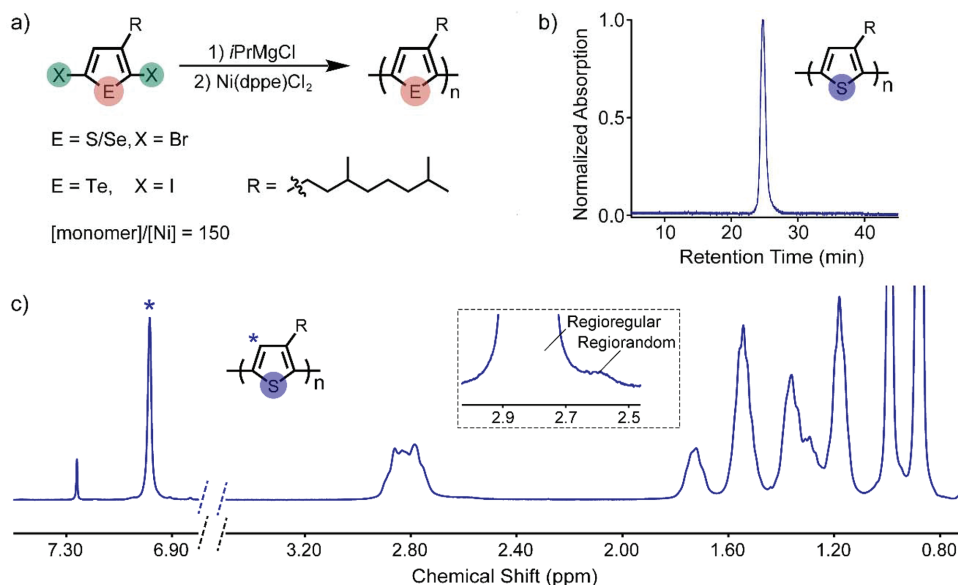


Figure 1. a) Synthetic scheme of the three regioregular poly(3-alkylchalcogenophene)s used in this study. R represents the 3,7-dimethyloctyl alkyl chain. Full synthetic details can be found in Supporting Information. b) GPC elution profile of PTh in 1,2,4-trichlorobenzene at 140 °C. c) ¹H NMR spectrum of PTh in CDCl₃.

reaction, which couples two monomer molecules.^[23] The ¹H NMR spectrum of **PTh** (Figure 1c) shows one aromatic singlet at 6.98 ppm corresponding to the protons on the polymer backbone. The high regioregularity of the three polymers (over 96%) is confirmed by the relative intensity of the two spectroscopically distinct regioregular and regiorandom methylene signals.

Optical and electrochemical characterizations reveal clear differences in polymer properties. Consistent with previous literature reports,^[18a,24] heavy atoms are found to decrease the optical band-gap, resulting in red-shifted absorption onsets (Figure S5, Supporting Information). This change in optical properties results from a combination of increased electron affinity and decreased ionization potential.^[25] Ionization potential is found to vary from 5.32 eV for **PTh**, to 5.26 eV for **PSe**, and 5.14 eV for **PTe**, as determined by cyclic voltammetry (Figure S6, Supporting Information).

Transistors based on the individual polymers exhibit distinct hole transport behavior. **Figure 2** displays the output and transfer characteristics of devices based on **PTh**, **PSe** and **PTe** spin-cast from a toluene solution with a concentration of 15 mg mL⁻¹. The drain current of the transistors continuously increases with larger mass of the heteroatom in the five-membered ring. The shape of the output curves in the low V_{ds} regime indicated higher contact resistance with increasing mass of the heteroatoms (Figure 2). Accordingly, the absolute values of the threshold voltage increased from 0.14 V for **PTh** up to -17.0 V for **PTe** (Table 1). The OFETs showed a small gate leakage and negligible hysteresis (Figure S9, Supporting Information). The square root of the drain current in the transfer characteristics of the OFETs with **PTh** and **PSe** showed a deviation from the ideal linear shape (Figure S7, Supporting Information). This behavior indicates a dependency of the charge carrier mobility

on the charge carrier density. When the gate voltage increases, more deep-trap states are filled and, as a result, the transport activation energy decreases resulting in a noticeable increase of the mobility.^[26] In the case of OFETs with **PTe**, the transfer characteristics revealed an almost ideal behavior indicating less charge carrier trapping. To evaluate charge carrier mobility and avoid overestimation, a narrow V_{gs} region from -20 to -40 V was chosen for the straight-line fitting on the $I_{ds}^{1/2}/V_{gs}$ plots for all three polymers (Figure S7, Supporting Information) (details provided in the Experimental Section). The charge carrier mobilities of **PTh** and **PSe** are within an order of magnitude whereas **PTe** is nearly three orders of magnitude larger than **PTh**. Correspondingly, the charge carrier mobilities are $\mu_h = 6.2 \times 10^{-5} \text{ cm}^2 \text{ V}^{-1} \text{ s}^{-1}$ for **PTh** and $8.0 \times 10^{-4} \text{ cm}^2 \text{ V}^{-1} \text{ s}^{-1}$ for **PSe** to $\mu_h = 2.5 \times 10^{-2} \text{ cm}^2 \text{ V}^{-1} \text{ s}^{-1}$ for **PTe**. The threshold voltage and the on/off ratio are also enhanced in the heavy analogues as summarized in Table 1. Since the non-ideal behavior of the transfer characteristics typically leads to an incorrect estimation of the charge carrier mobility, a comprehensive analysis of the transistor data was performed to confirm the improved device performance for **PTe**. Firstly, the charge carrier mobility in both saturation and linear regimes was plotted as function of the gate voltage (V_{gs}) (Figure S8, Supporting Information). It proved that for any given V_{gs} , the mobility significantly increased with the mass of the heteroatom in the order **PTh** < **PSe** < **PTe**. The mobility of **PTh** and **PSe** continuously raised with increasing V_{gs} over the whole measured V_{gs} regime, while a saturation was noticed for **PTe** above approx. -25 V. This behavior is characteristic for a more ideal device operation of **PTe**. Based on recent literature, the reliability factors and effective carrier mobilities were also determined (see details in the Experimental section). The reliability factor indicates the

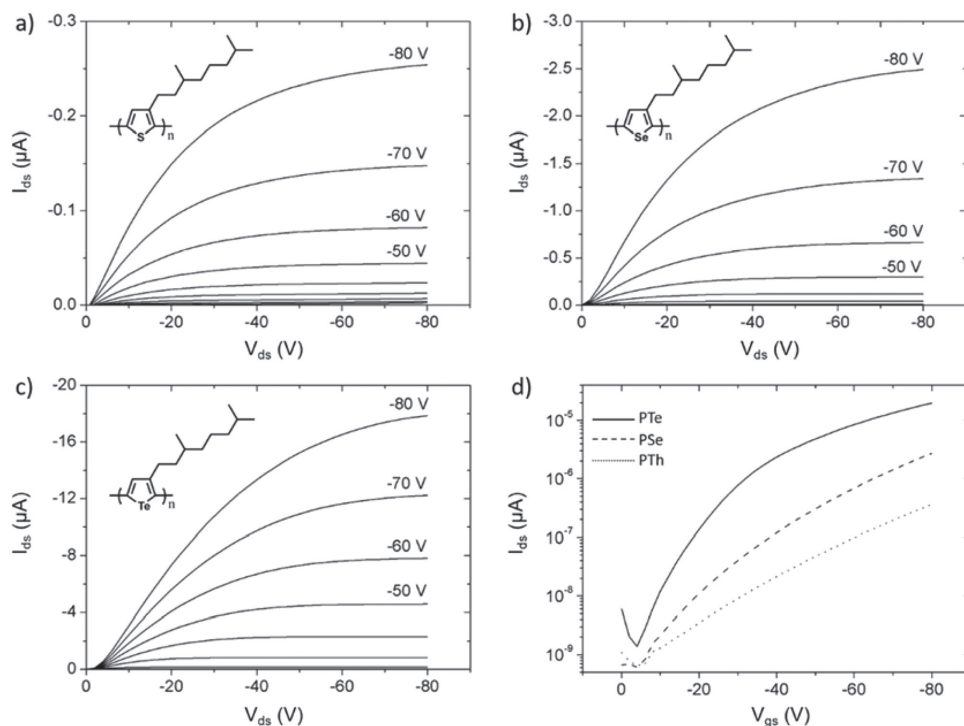


Figure 2. Output characteristics of FETs based on a) **PTh**, b) **PSe**, and c) **PTe**; d) transfer characteristics of all three polymers.

Table 1. Average charge carrier mobility with standard deviation, reliability factor, effective charge carrier mobility, threshold voltage, and on/off ratio for transistors based on spin-coated **PTh**, **PSe**, and **PTe** films.

Polymer	μ_h [$\text{cm}^2 \text{V}^{-1} \text{s}^{-1}$]	Reliability factor r	$\mu_{\text{effective}}$ [$\text{cm}^2 \text{V}^{-1} \text{s}^{-1}$]	V_{th} [V]	On/off
PTh	6.2×10^{-5} ($\pm 0.5 \times 10^{-5}$)	4.3	2.7×10^{-4}	0.14	210
PSe	8.0×10^{-4} ($\pm 2 \times 10^{-4}$)	2.6	2.1×10^{-3}	-14	4000
PTe	2.5×10^{-2} ($\pm 0.2 \times 10^{-2}$)	0.5	1.6×10^{-2}	-17	11 000

deviation from an ideal transistor operation and the effective carrier mobility provides the charge transporting properties of an electrically equivalent device with the same maximum drain currents, but without the non-linear behavior of the transfer characteristics. The shape of the $I_{\text{ds}}^{1/2}/V_{\text{gs}}$ plots for these theoretically ideal OFETs are indicated as dashed lines in Figure S7, Supporting Information. The calculated effective mobilities of OFETs with **PTh** and **PSe** are higher than determined from the transfer curves (Table 1). However, the effective mobility of **PTe** is still almost an order of magnitude higher than for **PSe** and almost two orders of magnitudes higher than **PTh**, which further confirms the enhancement in charge transport. The electrical results from the transistor measurements imply that embedding heavier atoms in the five-membered rings of a conjugated polymer improves the charge carrier transport. While the **PTe** values are similar to P3HT,^[27] it should be noted that all of these polymers have branched side groups, and this dramatically decreases the mobility of the sample,^[28] for example P3EHT has a mobility of around $1 \times 10^{-5} \text{ cm}^2 \text{V}^{-1} \text{s}^{-1}$.^[27] In light of this, a value of $\mu_h = 2.5 \times 10^{-2} \text{ cm}^2 \text{V}^{-1} \text{s}^{-1}$ for **PTe** indicates that heavy atom substitution leads to high mobility in spite of potentially problematic branched side chains.

Interestingly, charge carrier mobility of **PTe** with DMO side chains is three orders of magnitude higher when compared with polymers bearing 2-ethylhexyl side chains.^[16a] The 2-ethylhexyl side chain was reported to be detrimental for the synthesis of this type of polymer,^[18b] leading to fairly low molecular weights (Table S2, Supporting Information), which has been shown to decrease the charge carrier mobility of conjugated polymers.^[19b] Previous reports found that alkyl chains with branch points closer to the heterocycle result in a more twisted polymer backbone.^[18b] The shorter and more distant branch in DMO side chain improves the polarity of the polymer

backbone as well. In summary, the 3,7-dimethyloctyl side chain enables highly controlled polymerizations and yields solution processable polymers with improved charge carrier mobility.

The polymer packing and crystallinity were investigated in both bulk and thin films. For the bulk measurements, macroscopically oriented fiber samples were prepared by extrusion and after annealing at 90 °C placed vertically in front of a two-dimensional wide-angle X-ray scattering (2DWAXS) detector (Figure 3).^[29] The annealing temperature was below the melting point of **PTh** and **PSe** (Figure S10, Supporting Information). Polymer **PTe** did not undergo any phase transition within the investigated temperature range. The patterns in Figure 3 reveal distinct differences between the three polymers. In all three fiber specimens, the polymer chains are aligned along the extrusion direction as evident from the small-angle equatorial 100 reflections. From these scattering intensities, the interlayer distance is derived as 2.30 nm for **PTh**, 2.26 nm for **PSe** and 1.92 nm for **PTe**. The smaller interlayer distance in heavier analogous polychalcogenophenes with an identical side chain (**PTh** > **PSe** > **PTe**) has been previously observed by us and others and is related to the polymer packing within the layers.^[11,18a,30] Specifically, the large heteroatom is thought to increase the π -stacking distance which allows more side chain interdigitation and decrease the interlayer distance. Remarkably enough, **PTe** does not show any higher order or π -stacking reflections which suggests poor order (Figure 3c). In contrast, the large number of reflections suggests high crystallinity for **PTh** (Figure 3a), while it slightly decreases for **PSe** (Figure 3b). Both polymers also reveal π -stacking with a distance of 0.37 nm for **PTh** and 0.38 nm for **PSe**.

The thin film organization of the polymers was further explored by grazing incidence wide-angle X-ray scattering (GIWAXS) which confirmed the differences in order observed for the bulk extruded samples (Figure 4). The highest crystallinity is found for **PTh** and the lowest for **PTe**. The main surface arrangement for the three polymers is assigned to edge-on as evident by the strong out-of-plane reflections related to the interlayer organization. The interlayer distance in thin films is in a similar range as in the bulk with 2.19 nm for **PTh**, 2.24 nm for **PSe** and 1.91 nm for **PTe** (Figure S11a, Supporting Information). Similarly, π -stacking is only observed for **PTh** (0.36 nm) and **PSe** (low intensity reflection, 0.37 nm), while **PTe** shows no packing of polymer chains within the layer structures. Interestingly, in **PTh**, besides the edge-on arrangement, the coexistence

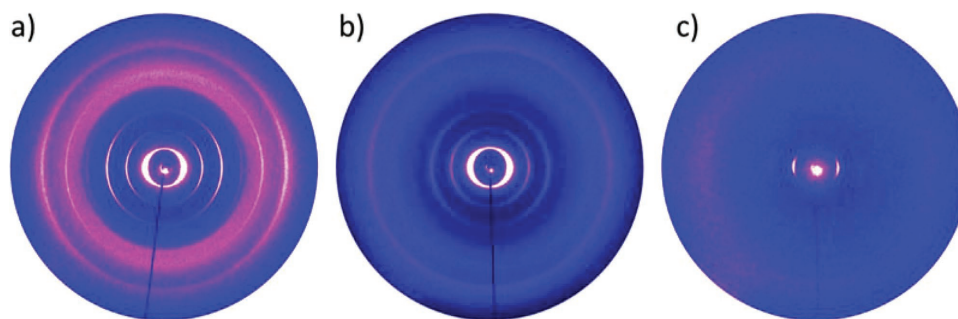


Figure 3. 2DWAXS patterns recorded at 30 °C for fiber specimens after annealing at 90 °C of a) **PTh**, b) **PSe**, and c) **PTe**.

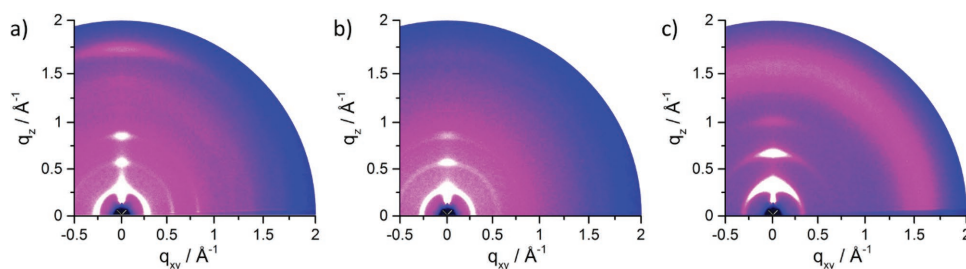


Figure 4. GIWAXS patterns recorded for films of a) PTh, b) PSe, and c) PTe.

of a face-on phase is evident from the out-of-plane π -stacking and additional in-plane interlayer reflections (Figure S11b, Supporting Information).^[31]

To better understand the origin of these different microstructures, surface topologies were analyzed by AFM. The thin films of the polymers that were used in FET studies all exhibit a similar nodular morphology by AFM (Figure 5), which is typical for thin films of conjugated polymers.^[32] However, slight differences were discerned between the film of PTe (Figure 5c) and those of the other two polymers (Figure 5a,b). Films obtained from PTe revealed a morphology consisting of small and dense globular features, whereas no such microstructure was observed in the other films. In these globular structures, the relatively poorly soluble polymer was quite disordered. The reduced solubility complicates solution processing and disrupts polymer packing, consistent with decreased π -stacking in PTe. Given that PSe exhibited a mobility that was more than a factor of 10 greater than PTh, but no distinct difference could be observed in the film microstructures, the AFM determined surface morphology appears insignificant.

To rationalize the dependence of mobility on the chemical structure of the polymer chain, a series of theoretical calculations were carried out. We first calculated ionization potential and electron affinities of corresponding tetramers. For all polymers, the variation of IPs and EAs is small (Table S3, Supporting Information) as confirmed experimentally by cyclic voltammetry.^[33] Hence the change in mobility cannot be attributed to a drastically different HOMO level or different injection barrier (Scheme S2, Supporting Information).

We then evaluated the energy profile of a rotation about the inter-ring bond (Figure 6). The simulations show that the relative stability of the cis conformation increases with heteroatom size, suggesting more cis conformers along the respective

polymer chains. This is consistent with the lower crystallinity of heavier polychalcogenophenes, particularly polytellurophene. Additionally, the rotational barrier gradually increases. A higher rotational barrier increases the difficulty in removing the conformational defects during processing resulting in their higher density along the backbone. This is evident from the increase in full width at half-maximum in the absorption spectra (Figure S5, Supporting Information).^[34] Most importantly, the large rotational barrier indicates that internal rotation in the tellurophene-based polymer (PTe) is more confined than in selenophene (PSe) and thiophene (PTh) analogues, leading to higher intrachain charge carrier mobility. The torsion angle between two repeat units decreases in the heavier analogues (Table S4, Supporting Information), indicating that the polymer chains are more planar. Again, the increasing planarity improves intrachain carrier transport. The more confined and planar backbone is consistent with the higher A_{00}/A_{01} transition observed in the absorption spectra of PTe (Figure S5, Table S5, Supporting Information), which can be interpreted as an increase in conjugation length and better intrachain order.^[35] Overall, our findings suggest that heavy atoms increase rotational barriers and planarity, ensuring higher carrier mobility even in low-crystallinity polymers.^[36]

A series of regioregular, high molecular weight, low dispersity poly(3-alkylchalcogenophene)s (S, Se, Te) has been prepared. A 3,7-dimethyloctyl side chain imparts similar processability to all three samples. The charge carrier mobility in transistors increases from PTh to PSe to PTe. PTh and PSe have similar surface morphology whereas PTe shows unique features. X-ray scattering reveals that the crystallinity of the samples follows the opposite trend in mobility. Importantly, we find that the increased torsional barrier and planarity conferred by heavier heteroatoms imparts high mobility despite the presence

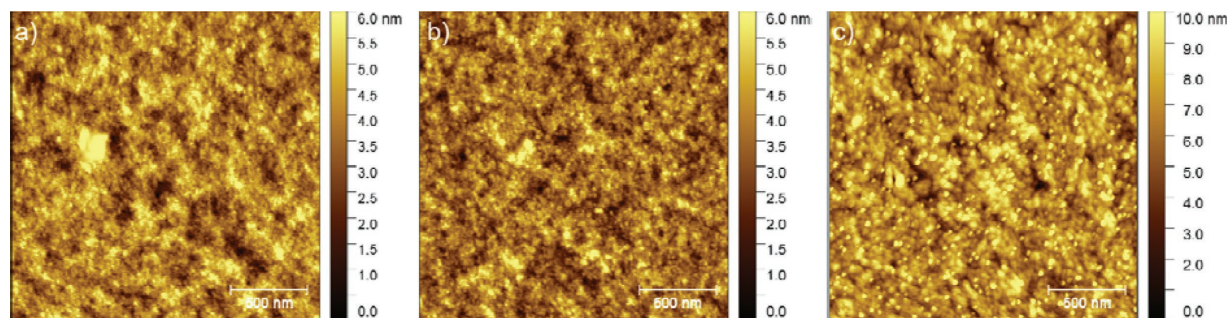


Figure 5. AFM height images of a) PTh, b) PSe, and c) PTe films.

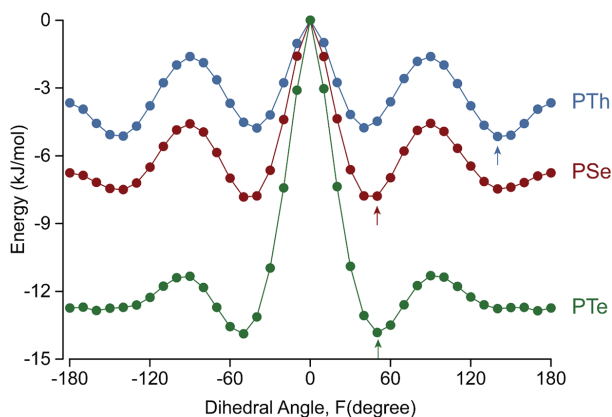


Figure 6. Dihedral potential between two neighboring repeat units calculated at B3LYP/6-31g+(d,p) level of theory (arrows indicate the lowest energy conformation).

of larger, branched alkyl chains. The results improve our understanding of “heavy” group-16 containing polymers and further support that high degrees of crystallinity are not necessary for high performance in FETs.

Experimental Section

Synthesis: Monomers were prepared according to literature procedures^[18b] starting with commercially available 3,7-dimethyl-1-octanol (Scheme S1, Supporting Information).

General Procedure for Polymerizations: Isopropylmagnesium chloride (0.98 equiv.) was added to a solution of 2,5-diiodo-3-(3,7-dimethyloctyl) tellurophene (350 mg, 0.61 mmol) in THF (5.2 mL). The mixture was stirred at r.t. for 15 min and then transferred to a Schlenk flask containing Ni(dppe)Cl₂ catalyst (2.16 mg, 0.0041 mmol, 0.67 mol%) and stirred at 40 °C for 1 h before quenching with dilute HCl. The polymer was precipitated into methanol and purified by sequential Soxhlet extraction (methanol, hexanes, and chloroform). The chloroform fraction was concentrated under reduced pressure to give a dark purple solid (113 mg, 58%). The polymer was further purified by column chromatography in chloroform before use.

Cyclic Voltammetry: Cyclic voltammetry measurements were conducted with a BASi Epsilon potentiostat on drop-cast polymer films (10 mg mL⁻¹ in CHCl₃) on gold electrodes. Measurements were run in acetonitrile/tetrabutylammonium hexafluorophosphate (0.1 M) solutions versus Ag/AgCl at a scan rate of 100 mV s⁻¹ with Fc/Fc⁺ as an internal reference. The onset values were determined using the intersection of the baseline with the steepest tangent to the curve.

Ultraviolet-Visible Spectroscopy: Optical absorption spectra of polymer thin films were obtained using a Varian Cary 5000 spectrometer. Glass slides were cleaned with aqueous detergent, thoroughly rinsed and washed in deionized water, acetone, and isopropanol for 15 min cycles in an ultrasonic bath. Slides were dried with pressurized nitrogen and treated with oxygen plasma for 10 min. Thin films were prepared by spin casting polymer solutions (10 mg mL⁻¹ in chlorobenzene stirred at 70 °C for 3 h) on clean glass slides at 2000 rpm for 30 s. Solutions were filtered through 0.45 μm PTFE syringe filters before deposition. Spectra were recorded on films annealed at 100 °C for 10 min in a nitrogen glovebox at <5 ppm O₂.

Charge Transport Measurements: Silicon substrates with a 300 nm silicon dioxide dielectric layer were used for the fabrication of field-effect transistors (FETs) using each polymer as the active material. Substrates were successively washed in acetone and isopropanol respectively for 15 min cycles in an ultrasonic bath. After drying with compressed

nitrogen, the substrates were treated with oxygen plasma for 5 min. Finally, the substrates were functionalized with hexamethyldisilazane (HMDS) vapor at 140 °C for 6 h. Substrates were then transferred to a nitrogen glove-box system. All FET fabrication and measurement was performed under inert atmosphere. All three polymers, PTH, PSe, and PTe, were dissolved in toluene at a concentration of 15 mg mL⁻¹ and stirred at 75 °C for 3 h. Solutions of other solvents such as chlorobenzene (CB) or 1,2-dichlorobenzene (DCB) were also prepared, but no continuous layers were obtained on HMDS functionalized substrates. OFETs prepared from CB and DCB solutions on untreated substrates exhibited a poor field-effect and are not included in this work. The semiconducting films were obtained by spin-coating at 3000 rpm for 2 min. After deposition, the films were annealed at 90 °C for 10 h in vacuum. Subsequently, gold source and drain top electrodes were thermally evaporated through a shadow mask to ensure the same configuration for all transistors. The channel dimensions of the bottom gate and top contact devices were 30 μm and 1 mm in length and width, respectively. The output and transfer characteristics were measured with needle micromanipulators connected to a Keithley 2636b electrometer. The charge carrier mobilities were calculated from transfer characteristics in the saturation regime, using the following formula:

$$I_d = \frac{W}{2L} C_i \mu (V_g - V_{th})^2$$

FETs based on PSe and PTH exhibited nonlinear behavior of the drain current in the transfer characteristics, especially for high gate voltages (Figure S7, Supporting Information). This may be the result of non-Ohmic contacts or charge trapping and scattering at the interface.^[37] A linear fit to the square root of the transfer curve in the region of high gate voltages would result in significantly overestimated values of the threshold voltages. Therefore, the parameters were extracted from the linear fit in the range between -20 and -40 V of the gate voltage. Non-ideal behavior of the OFETs, expressed as a deviation from the linearity of the transfer characteristics, causes ambiguity in the mobility estimations. To provide more information on the charge carrier mobility in saturation and linear regimes, a relation between the mobility and gate voltage was derived as shown in Figure S8, Supporting Information. Mobility in the linear region was calculated from the transfer curves at V_{ds} = -20 V, according to the following formula:

$$I_d = \frac{W}{L} C_i \mu_{lin} (V_g - V_{th}) V_{ds}$$

Effective mobilities were calculated according to recent literature.^[38] This parameter describes an equivalent electrical performance of a device in which the relation between drain current and gate voltage would follow the ideal (linear) pattern. The calculation of the effective carrier mobility is based on the following formula:

$$\mu_{eff} = r \times \mu_{claimed}$$

where $\mu_{claimed}$ stands for the mobility calculated by fitting the straight line to the chosen region of the $I_{ds}^{1/2}/V_{gs}$ relation and r is the reliability factor (the closer this factor is to the value of 1, the more ideal is the behavior of the OFET). The reliability factor is calculated according to the following formula:

$$r = \frac{\left(\frac{\sqrt{|I_{ds}|^{max}} - \sqrt{|I_{ds}|^0}}{|V_G|^{max}} \right)^2}{\left(\frac{\partial \sqrt{|I_{ds}|}}{\partial V_G} \right)^2}$$

where $|I_{ds}|^{max}$ is the maximum source-drain current, $|I_{ds}|^0$ is the source-drain current at $V_G = 0$ V and $|V_G|^{max}$ is the maximum gate voltage.

Differential Scanning Calorimetry: Differential scanning calorimetry (DSC) was performed on a Mettler DSC 30 at a heating/cooling rate of 10 °C min⁻¹ under nitrogen flow.

Atomic Force Microscopy: Height imaging of the films was performed in tapping mode using a Nanoflex atomic force microscope (AFM). All images were obtained with Olympus silicon cantilevers at 320 kHz resonance frequency.

X-Ray Scattering: 2DWAXS measurements of the thin films were performed using a custom setup consisting of a copper solid-anode X-ray tube (Bruker AXS Krystalloflex 760, operated at 35 kV and 30 mA), Osmic confocal MaxFlux optics and a three pin-hole collimation system. The X-ray beam size has 1.0 mm radius. The samples were prepared as a thin filament, 0.7 mm in diameter, via filament extrusion at 25 °C using a custom-built miniextruder.^[39] For the measurements, the samples were firstly annealed at 90 °C below the melting point of PTh and PSe and then positioned perpendicular to the incident X-ray beam and vertical to the 2D detector. The scattering intensity was detected on a 2D image plate (MAR-345) with a pixel size of 100 μm (2345 × 2345 pixels), and the detector was placed 300 mm from the sample center. Scattering data are expressed as a function of the scattering vector: $q = 4\pi/\lambda \sin\theta$, where θ is half the scattering angle and $\lambda = 0.154$ Å is the wavelength of the incident radiation. GIWAXS measurements of thin films were performed using the same equipment. For thin films, the samples were irradiated just below the critical angle for total reflection with respect to the incoming X-ray beam ($\approx 0.1^\circ$). All X-ray scattering measurements were performed under vacuum (≈ 20 mbar) to reduce air scattering and beam damage to the samples. All 2DWAXS data processing and analysis was performed using the software package Datasqueeze (<http://www.datasqueezesoftware.com>).

Supporting Information

Supporting Information is available from the Wiley Online Library or from the author.

Acknowledgements

S.Y. and L.J. contributed equally to this work. W.P. acknowledges the National Science Centre, Poland, through the grant UMO-2015/18/E/ST3/00322. D.S.S. is grateful from support from the NSERC of Canada.

Conflict of Interest

The authors declare no competing financial interest.

Keywords

crystallinity, field-effect transistors, polyselenophene, polytellurophene, polythiophene

Received: August 7, 2018

Revised: October 3, 2018

Published online:

[1] H. Sirringhaus, *Adv. Mater.* **2014**, *26*, 1319.

[2] H. Sirringhaus, P. J. Brown, R. H. Friend, M. M. Nielsen, K. Bechgaard, B. M. W. Langeveld-Voss, A. J. H. Spiering, R. A. J. Janssen, E. W. Meijer, P. Herwig, D. M. de Leeuw, *Nature* **1999**, *401*, 685.

- [3] J. Liu, R. Zhang, G. Sauvé, T. Kowalewski, R. D. McCullough, *J. Am. Chem. Soc.* **2008**, *130*, 13167.
- [4] M. Zhang, H. N. Tsao, W. Pisula, C. Yang, A. K. Mishra, K. Müllen, *J. Am. Chem. Soc.* **2007**, *129*, 3472.
- [5] Y. Li, P. S. Samarendra, P. Sonar, *Adv. Mater.* **2010**, *22*, 4862.
- [6] S. Y. Son, Y. Kim, J. Lee, G.-Y. Lee, W.-T. Park, Y.-Y. Noh, C. E. Park, T. Park, *J. Am. Chem. Soc.* **2016**, *138*, 8096.
- [7] R. Noriega, J. Rivnay, K. Vandewal, F. P. V. Koch, N. Stingelin, P. Smith, M. F. Toney, A. Salleo, *Nat. Mater.* **2013**, *12*, 1038.
- [8] T. Yokozawa, Y. Ohta, *Chem. Rev.* **2016**, *116*, 1950.
- [9] K. Müllen, W. Pisula, *J. Am. Chem. Soc.* **2015**, *137*, 9503.
- [10] W. Li, L. Yang, J. R. Tumbleston, L. Yan, H. Ade, W. You, *Adv. Mater.* **2014**, *26*, 4456.
- [11] M. Heeney, W. Zhang, D. J. Crouch, M. L. Chabiny, S. Gordeyev, R. Hamilton, S. J. Higgins, I. McCulloch, P. J. Skabara, D. Sparrowe, S. Tierney, *Chem. Commun.* **2007**, *0*, 5061.
- [12] a) S. M. Parke, M. P. Boone, E. Rivard, *Chem. Commun.* **2016**, *52*, 9485; b) M. Jeffries-EL, B. M. Kobilka, B. J. Hale, *Macromolecules* **2014**, *47*, 7253; c) C.-H. Tsai, A. Fortney, Y. Qiu, R. R. Gil, D. Yaron, T. Kowalewski, K. J. T. Noonan, *J. Am. Chem. Soc.* **2016**, *138*, 6798.
- [13] J. Hollinger, D. Gao, D. S. Seferos, *Isr. J. Chem.* **2014**, *54*, 440.
- [14] a) Y.-J. Hwang, T. Earmme, B. A. E. Courtright, F. N. Eberle, S. A. Jenekhe, *J. Am. Chem. Soc.* **2015**, *137*, 4424; b) R. S. Ashraf, I. Meager, M. Nikolka, M. Kirkus, M. Planells, B. C. Schroeder, S. Holliday, M. Hurhangee, C. B. Nielsen, H. Sirringhaus, I. McCulloch, *J. Am. Chem. Soc.* **2015**, *137*, 1314.
- [15] a) M. Al-Hashimi, Y. Han, J. Smith, H. S. Bazzi, S. Y. A. Alqaradawi, S. E. Watkins, T. D. Anthopoulos, M. Heeney, *Chem. Sci.* **2016**, *7*, 1093; b) M. Kaur, D. S. Yang, J. Shin, T. W. Lee, K. Choi, M. J. Cho, D. H. Choi, *Chem. Commun.* **2013**, *49*, 5495; c) D. J. Crouch, P. J. Skabara, M. Heeney, I. McCulloch, D. Sparrowe, S. J. Coles, M. B. Hursthouse, *Macromol. Rapid Commun.* **2008**, *29*, 1839.
- [16] a) A. A. Jahnke, L. Yu, N. Coombs, A. D. Scaccabarozzi, A. J. Tilley, P. M. DiCarmine, A. Amassian, N. Stingelin, D. S. Seferos, *J. Mater. Chem. C* **2015**, *3*, 3767; b) J. Razzell-Hollis, F. Fleischli, A. A. Jahnke, N. Stingelin, D. S. Seferos, J.-S. Kim, *J. Phys. Chem. C* **2017**, *121*, 2088.
- [17] A. A. Jahnke, D. S. Seferos, *Macromol. Rapid Commun.* **2011**, *32*, 943.
- [18] a) A. A. Jahnke, B. Djukic, T. M. McCormick, E. B. Domingo, C. Hellmann, Y. Lee, D. S. Seferos, *J. Am. Chem. Soc.* **2013**, *135*, 951; b) S. Ye, M. Steube, E. I. Carrera, D. S. Seferos, *Macromolecules* **2016**, *49*, 1704.
- [19] a) R. J. Kline, M. D. McGehee, E. N. Kadnikova, J. Liu, J. M. J. Fréchet, M. F. Toney, *Macromolecules* **2005**, *38*, 3312; b) A. G. Dixon, R. Visvanathan, N. A. Clark, N. Stingelin, N. Kopidakis, S. E. Shaheen, *J. Polym. Sci., Part B: Polym. Phys.* **2018**, *56*, 31.
- [20] M. Wong, J. Hollinger, L. M. Kozycz, T. M. McCormick, Y. Lu, D. C. Burns, D. S. Seferos, *ACS Macro Lett.* **2012**, *1*, 1266.
- [21] a) R. J. Kline, M. D. McGehee, E. N. Kadnikova, J. Liu, J. M. J. Fréchet, *Adv. Mater.* **2003**, *15*, 1519; b) P. Schilinsky, U. Asawapirom, U. Scherf, M. Biele, C. J. Brabec, *Chem. Mater.* **2005**, *17*, 2175; c) F. Panzer, H. Bässler, R. Lohwasser, M. Thelakkat, A. Köhler, *J. Phys. Chem. Lett.* **2014**, *5*, 2742; d) L. Lu, T. Zheng, T. Xu, D. Zhao, L. Yu, *Chem. Mater.* **2015**, *27*, 537.
- [22] a) T. Adachi, J. Brazard, R. J. Ono, B. Hanson, M. C. Traub, Z.-Q. Wu, Z. Li, J. C. Bolinger, V. Ganesan, C. W. Bielawski, D. A. Vanden Bout, P. F. Barbara, *J. Phys. Chem. Lett.* **2011**, *2*, 1400; b) X. Jiang, Y. Harima, K. Yamashita, Y. Tada, J. Ohshita, A. Kunai, *Synth. Met.* **2003**, *135–136*, 351.
- [23] R. Miyakoshi, A. Yokoyama, T. Yokozawa, *J. Am. Chem. Soc.* **2005**, *127*, 17542.
- [24] G. Li, L. Xu, W. Zhang, K. Zhou, Y. Ding, F. Liu, X. He, G. He, *Angew. Chem., Int. Ed.* **2018**, *57*, 4897.
- [25] E. I. Carrera, D. S. Seferos, *Macromolecules* **2015**, *48*, 297.



- [26] H. Bäessler, A. Köhler, *Top. Curr. Chem.* **2012**, 312, 1.
- [27] H. Luo, C. Yu, Z. Liu, G. Zhang, H. Geng, Y. Yi, K. Broch, Y. Hu, A. Sadhanala, L. Jiang, P. Qi, Z. Cai, H. Sirringhaus, D. Zhang, *Sci. Adv.* **2016**, 2, e1600076.
- [28] B. Burkhardt, P. P. Khlyabich, B. C. Thompson, *Macromolecules* **2012**, 45, 3740.
- [29] C. R. G. Grenier, W. Pisula, T. J. Joncheray, K. Müllen, J. R. Reynolds, *Angew. Chem., Int. Ed.* **2007**, 46, 714.
- [30] L. Li, J. Hollinger, A. A. Jahnke, S. Petrov, D. S. Seferos, *Chem. Sci.* **2011**, 2, 2306.
- [31] X. Guo, S. R. Puniredd, M. Baumgarten, W. Pisula, K. Müllen, *J. Am. Chem. Soc.* **2012**, 134, 8404.
- [32] H. N. Tsao, K. Müllen, *Chem. Soc. Rev.* **2010**, 39, 2372.
- [33] J. G. Manion, S. Ye, A. H. Proppe, A. W. Laramée, G. R. McKeown, E. L. Kynaston, S. O. Kelley, E. H. Sargent, D. S. Seferos, *ACS Appl. Energy Mater.* **2018**, 1, 5033.
- [34] A. Thiessen, J. Vogelsang, T. Adachi, F. Steiner, D. Vanden Bout, J. M. Lupton, *Proc. Natl. Acad. Sci. USA* **2013**, 110, E3550.
- [35] a) J. Clark, J.-F. Chang, F. C. Spano, R. H. Friend, C. Silva, *Appl. Phys. Lett.* **2009**, 94, 163306; b) J. Clark, C. Silva, R. H. Friend, F. C. Spano, *Phys. Rev. Lett.* **2007**, 98, 206406; c) J.-F. Chang, J. Clark, N. Zhao, H. Sirringhaus, D. W. Breiby, J. W. Andreasen, M. M. Nielsen, M. Giles, M. Heeney, I. McCulloch, *Phys. Rev. B* **2006**, 74, 115318.
- [36] a) D. Venkateshvaran, M. Nikolka, A. Sadhanala, V. Lemaire, M. Zelazny, M. Kepa, M. Hurhangee, A. J. Kronemeijer, V. Pecunia, I. Nasrallah, I. Romanov, K. Broch, I. McCulloch, D. Emin, Y. Olivier, J. Cornil, D. Beljonne, H. Sirringhaus, *Nature* **2014**, 515, 384; b) G. L. Schulz, F. S. U. Fischer, D. Trefz, A. Melnyk, A. Hamidi-Sakr, M. Brinkmann, D. Andrienko, S. Ludwigs, *Macromolecules* **2017**, 50, 1402; c) C. Poelking, D. Andrienko, *Macromolecules* **2013**, 46, 8941; d) C. Poelking, K. Daoulas, A. Troisi, D. Andrienko, *In P3HT Revisited-From Molecular Scale to Solar Cell Devices*, (Ed: S. Ludwigs), Springer, Berlin **2014**, p. 139.
- [37] G. Nisato, D. Lupo, S. Ganz, *Organic and Printed Electronics: Fundamentals and Applications*, CRC Press, Boca Raton, FL, **2016**.
- [38] H. H. Choi, K. Cho, C. D. Frisbie, H. Sirringhaus, V. Podzorov, *Nat. Mater.* **2018**, 17, 2.
- [39] W. Pisula, Z. Tomovic, C. Simpson, M. Kastler, T. Pakula, K. Müllen, *Chem. Mater.* **2005**, 17, 4296